Ultra-widefield photoacoustic microscopy with a dual-channel slider-crank laser-scanning apparatus for *in vivo* biomedical study

Van Tu Nguyen [a,1], Nguyen Thanh Phong Truong [a,1], Van Hiep Pham [a], Jaeyeop Choi [a,d], Sumin Park [a], Cao Duong Ly [a], Soon-Woo Cho [b], Sudip Mondal [c], Hae Gyun Lim [c], Chang-Seok Kim [b,**], Junghwan Oh [a,c,d,*]

[a] *Industry 4.0 Convergence Bionics Engineering, Pukyong National University, Republic of Korea*
[b] *Department of Cogno-Mechatronics Engineering, Pusan National University, Busan, 46241, Republic of Korea*
[c] *Department of Biomedical Engineering, Pukyong National University, Busan, 48513, Republic of Korea*
[d] *Ohlabs Corp, Busan, 48513, Republic of Korea*

ARTICLE INFO

ABSTRACT

Photoacoustic microscopy (PAM) is an important imaging tool that can noninvasively visualize the anatomical structure of living animals. However, the limited scanning area restricts traditional PAM systems for scanning a large animal. Here, we firstly report a dual-channel PAM system based on a custom-made slider-crank scanner. This novel scanner allows us to stably capture an ultra-widefield scanning area of 24 mm at a high B-scan speed of 32 Hz while maintaining a high signal-to-noise ratio. Our system's spatial resolution is measured at ~3.4 μm and ~37 μm for lateral and axial resolution, respectively. Without any contrast agent, a dragonfly wing, a nude mouse ear, an entire rat ear, and a portion of mouse sagittal are successfully imaged. Furthermore, for hemodynamic monitoring, the mimicking circulating tumor cells using magnetic contrast agent is rapidly captured *in vitro*. The experimental results demonstrated that our device is a promising tool for biological applications.

1. Introduction

Photoacoustic (PA) imaging is an emerging biomedical modality based on a PA effect [1], in which ultrasonic emission occurs when biological tissues absorb a short-pulsed laser. The emitted ultrasonic waves which are named by PA waves, are acquired by a transducer to construct PA images for multipurpose applications. The most common PA imaging is photoacoustic microscopy (PAM), which provides a micron-scale spatial resolution by focusing either the optical beam or acoustic beam. While optical-resolution PAM (OR-PAM) mechanism relies on a stronger optical focus, acoustic-resolution PAM (AR-PAM) [2] mechanism follows a stronger acoustic focus. Particularly, based on the much stronger and tighter optical beam than the acoustic beam, OR-PAM takes extreme advantage of the high resolution over AR-PAM. In addition, with the rich optical absorption contrast, OR-PAM becomes a promising imaging tool in many research fields including biology, dermatology, neurology, oncology, ophthalmology, and pathology

[3–16]. Typical OR-PAM systems implement a confocal and coaxial structure of the excitation light beam and the PA emission beam to maximize the signal-to-noise ratio (SNR) and optimize the spatial resolutions [6,8,12,17]. Three-dimension imaging is typically formed by raster scanning of the PA probe over the sample by using the scanning stages [18–20]. Due to the micron-level lateral resolution, the OR-PAM required the fine step size leading to the long scanning time within a small scanning range [21,22]. Therefore, it is a limit of OR-PAM for achieving tissue's hemodynamic information, such as temporary drug responses and skin vasculature.

The present trends of OR-PAM imaging highly focused on the extended field of view (FOV) with reduced scanning time while maintaining a highly sensitive detection. Although the scanning time technically depends on the pulse repetition rate (PRR) of the laser and scanning mechanism, it is theoretically limited by the sound speed of the PA waves in biological tissues [23]. Several high-speed scanning techniques for OR-PAM have been reported, such as galvanometer scanner,

microelectromechanical system (MEMS) scanner, hexagon-mirror scanner, and voice-coil scanning system [8,24–30]. These scanners can be classified into two main mechanisms including mechanical scanning (voice-coil scanner) and optical scanning (the other scanners). Although each mechanism has its own advantages, there is no existing OR-PAM system that accomplishes all the optimal scanning features, including high resolution, good SNR, and fast scanning speed [30,31]. The galvanometer scanners have been reported to be appropriate for fast and steady scanning in traditional optical microscopy systems [26,32–37]. However, they have classically been employed in OR-PAM in optical scanning in air only, leading to non-alignment between optical beams and acoustic waves. Thus, these galvo-mirror-based optical scanning OR-PAMs have a relatively low SNR and/or a short scanning range within the spot size of the transducer. Therefore, the recent development of optical scanning system has employed a water-immersible mirror to simultaneously steer both focused the optical beams and emitted acoustic waves [8,26,28]. Although these OR-PAMs increase the B-scan rate up to ten of hundreds Hz with a relatively good SNR, the scanning range is still narrow. With the water-immersible mirror, there is no effective way to extend the FOV for a single scanning time. For instance, a semi-water-immersible galvanometer scanner increases the B-scan rate up to 500 Hz over a small FOV of ~2.4 mm [38]. With this limited FOV, the operator has to scan multiple images and then manually merge them during post-processing to achieve a larger image. Thus, it is not appropriate for scanning large-scale areas in clinical applications. Water-immersible MEMS scanners enable high-speed scanning up to 400 Hz for 1D and 50 Hz for 2D (with scanning ranges of 3 mm and 9 mm, respectively) [39]. Nevertheless, the FOV of these MEMS scanners substantially decreases to less than 1 mm, unless the scanner is driven at its resonant frequency. Moreover, MEMS scanners are also limited for long-term use by their vulnerability, and the rendered PA images are quite deformed due to the distorted scanning patterns. To expand the scanning range, a hexagon-mirror scanner has been used to achieve a B-scan speed of 900 Hz over a FOV of 12 mm [27]. However, due to the unequal step size, the quality of PA images is relatively not good, and interpolation of the raw data is required to reconstruct the final PA images. In addition, steering the laser and ultrasound beam leads to a curvature scanning plane which limits a large FOV imaging, such as the entire mouse sagittal. Furthermore, adding the steering mirror is the cause of long-distance travel of ultrasound and laser that increases the PA signal attenuation and loosens the lateral resolution [40]. Unlike water-immersible mirror scanning, mechanical scanning enables high-speed scanning with the high numerical aperture of optical and acoustic lens while maintaining the confocal and coaxial alignment of the optical and acoustic beams over a large flat plane. The voice-coil scanner is an effective mechanical approach at the high scanning speed of 40 B-scan/mm [29]. However, with increasing scanning speed, the voice-coil scanner's performance is hampered by its bulky scanning head that induces the vibration at the high driving force.

In this study, to overcome the aforementioned limitations, we first present a fast OR-PAM using a slider-crank mechanism with two channels (SC-2-OR-FPAM). The system utilizes the customized slider-crank mechanism with high accuracy and precise movement. Dual channels of OR-PAM are used to doubly increase the FOV in single scan. In addition, our system employs a linear encoder to positioning the two channels, thus the scanning step size, which is not depend on the angular motion, is constant. Therefore, the PA images are reconstructed by raw data without using another image processing method. Our SC-2-OR-FPAM system enables us to achieve a maximum B-scan rate of 32 Hz over an ultra-widefield scanning range of 24 mm with a high lateral resolution. To target the smaller sample, the imaging range of system can be programmatically switchable to 12.5 mm by using one channel. To evaluate the efficiency of the developed system, four different samples (such as a dragonfly wing, a nude mouse ear, an entire rat ear, and a mouse sagittal) with variable dimensions and thickness were studied for high-speed scanning. To study further the hemodynamic activity, the

rapid change of the mimicking circulating tumor cells (CTCs) was successfully monitored real-time using the magnetic contrast agent. These experimental results have demonstrated the promising application in preclinical SC-2-OR-FPAM imaging for biomedical imaging.

2. Materials and methods

2.1. The slider-crank fast-scanning system

Our slider-crank mechanism converts rotary motion to linear motion as in a reciprocating piston pump. A step rotary motor (PK546PMA-R28, Oriental Motor, Tokyo, Japan) was used as the rotary engine, and a linear guideway (HGW15CA1R62Z0C, HIWIN, Taichung, Taiwan) was used as a rail. Our mechanism used the linear encoder (SME21-L-1-1-I-L2-H, Lika Electronic, Carre, Italy) as a positioning module with the smallest step size at 1 μm. The counter balance weight was calculated to optimize the vibration of the system. The other mechanical parts were designed and fabricated using a milling machine (DNM 4500, Doosan, Seoul, Republic of Korea). A micro-controller (STM32F407VG, STMicroelectronics, Geneva, Switzerland) was used to control the motor and synchronize both linear encoder and laser to trigger the data acquisition system (DAQ) (PXI 5124, National Instruments, Austin, TX, USA). The weight of the scanner is about 1.2 kg with three dimensions of 170, 90, and 70 mm corresponding to the x-, y-, and z- axes.

2.2. The configuration of the SC-2-OR-FPAM

Fig. 1 is a schematic representation of the 2-OR-FPAM system (FPAM-200, Ohlabs Corp, Busan, Republic of Korea). A pulsed green nanosecond fiber laser (GLP-10, IPG Photonics Corporation, Oxford, MA, USA) was used as the excitation source. The laser energy can reach up to 20 μJ with a pulsed duration of ~1 ns and a maximum PRR of 600 kHz. First, the laser beam was split into two, and the energy ratio was adjusted by a first variable beam-splitter (VA5-532/M, Thorlabs, Newton, NJ, USA). One beam was coupled with a single-mode fiber (P3-460B-FC-2, Thorlabs, Newton, NJ, USA) to attach to the first PA probe. The other beam is split again by the second variable beam-splitter (VA5-532/M, Thorlabs, Newton, NJ, USA) into two beams. The newly split beam was coupled into a second single mode fiber (P3-460B-FC-2, Thorlabs, Newton, NJ, USA) for the second PA probe. Whereas, the other split beam was used as a trigger source for the photo detector (SM05PD2A, Thorlabs, Newton, NJ, USA) as described in Fig. 1. In the OR-PAM module (also see Supplementary Movie 1), the laser beam from the optical fiber is first collimated (F220APC, Thorlabs, Newton, NJ, USA) and then focused by an aspherical lens (A280TM-A, Thorlabs, Newton, NJ, USA). The optical-acoustic beam combiner (OAC) was made of two right-angled prisms (PS910 and MRA10-G01, Thorlabs, Newton, NJ, USA) and an acoustic lens (LC4291, Thorlabs, Newton, NJ, USA). The aluminum coating reflects the laser beam and allows the ultrasound to go through. The PA signal was collected by the flat ultrasonic transducer (V214-BC-RM, Olympus, Tokyo, JP) and then amplified by two amplifiers (ZFL 500 L N, Mini-Circuits, Brooklyn, NY, USA). The magnified signal was digitized by a 12-bit DAQ board at a sampling rate of 200 MS/s. To perform raster scanning, the PA probe was attached in the scanning system including slider-crank scanner for fast axis (x-direction) and linear motor stage (UTM100PP1HL, Newport, CA, USA) for slow axis (y-direction). In the FOV of 25 mm, there was an overlap of 0.5 mm of each channel leading to an actual FOV of 24 mm. A laser energy of 80 nJ per pulse was used for all *in vivo* experiments.

3. Results

3.1. Structure of the slider-crank scanner

The new slider-crank scanner consists of three main parts: a rotation motor with a counter balance, a linear slider guideway, and a PA probe
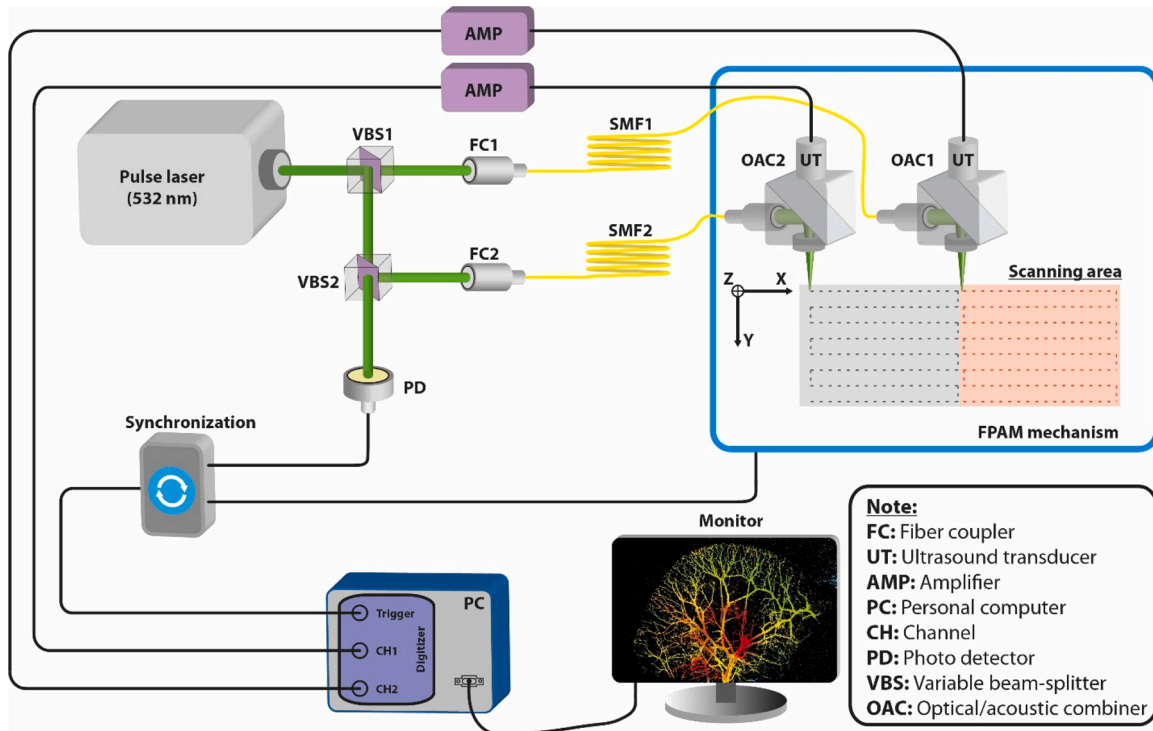
Fig. 1. The configuration of the CS-2-OR-FPAM system.

with two channels integrated with the positioning module. (as in Fig. 2). The scanning speed of our system is directly proportional to the torque force of the rotation motor, which is inversely proportional to the mass of the PA probe, as expected from Eq. (1):

$$\mathbf{T} = m\mathrm{d}, \tag{1}$$

where "**T**" is the torque of the motor, "d" is the distance between the rotation center point and the PA probe, and "m" is the mass of the PA probe. Therefore, to optimize the scanning speed, the housing for the PA probe was made from acrylic, and the other mechanical parts were designed and made from aluminum to minimize the total weight. Our new SC-2-OR-FPAM system can achieve a maximum B-scan speed of 44 Hz; however, the system works stably at the frequency of 32 Hz within the safe speed of the rotary motor. A full-scanning video (Supplementary Movie 2) shows the performance of our system at a B-scan rate of 26 Hz. The maximum scanning range in the *x*-direction was 25 mm, with a radius R of 12.5 mm (Fig. 2A), and the maximum imaging range in the *y*-direction was 100 mm. To form the image of two PA channels, 0.5 mm along the x-axis was used as an overlap area to align each channel. Therefore, the practical scanning range in the x-direction of our CS-2-OR-FPAM system was 24 mm.

3.2. Spatial resolution, penetration depth, and SNR of the CS-OR-2-FPAM system

To measure the lateral resolution of our system, we used the edge of a square chrome pattern on a USAF resolution target (R3DL3P, Thorlabs, Newton, NJ, USA) and obtained a PA maximum amplitude projection (MAP) image (Supplementary Fig. S1). The lateral resolutions were measured around 3.1 μm for channel 1 and 3.8 μm for channel 2, whereas the theoretical value is 1.8 μm (for an optical wavelength of 532 nm, a focal length of 16.7 mm, and beam diameter of 5 mm). The difference in lateral resolution between two channels is due to the error of different optical components. A carbon fiber with a 6 μm diameter was used to measure axial resolution. As illustrated in Fig. 3C and 3D, the measured axial resolutions were 39 μm for channel 1 and 35 μm for channel 2, whereas the theoretical value was approximately 33 μm. The possible reason for this difference could be the characteristic (for example the bandwidth) of two transducers. Furthermore, a PA image of the carbon fiber was also used for calculating the SNR. The laser energy was set for both channels at 6 nJ/pulse. Our results indicate that the calculated SNRs of channels 1 and 2 were similarly 23.05 dB and 23.61 dB, respectively. After analyzing the mouse ear PA image, the SNR of our PA system was calculated to be approximately 35.1 dB. The
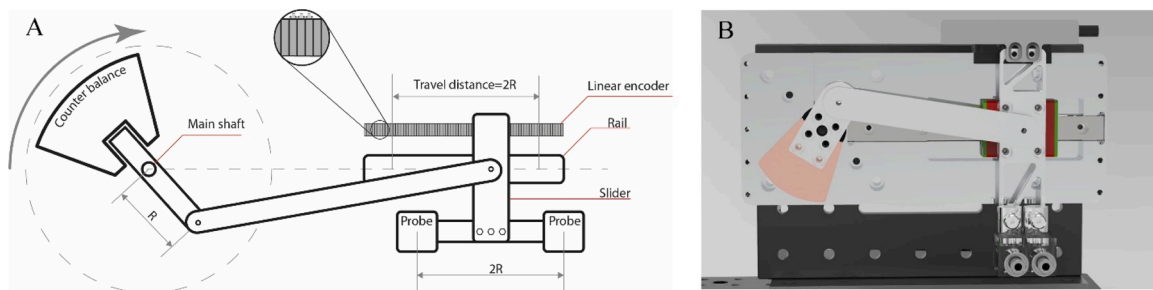

Fig. 2. Structure of slider-crank scanner of CS-2-OR-FPAM. (A) Schematic diagram of the slider-crank scanner. (B) The rendering photograph of the CS-2-OR-FPAM system.
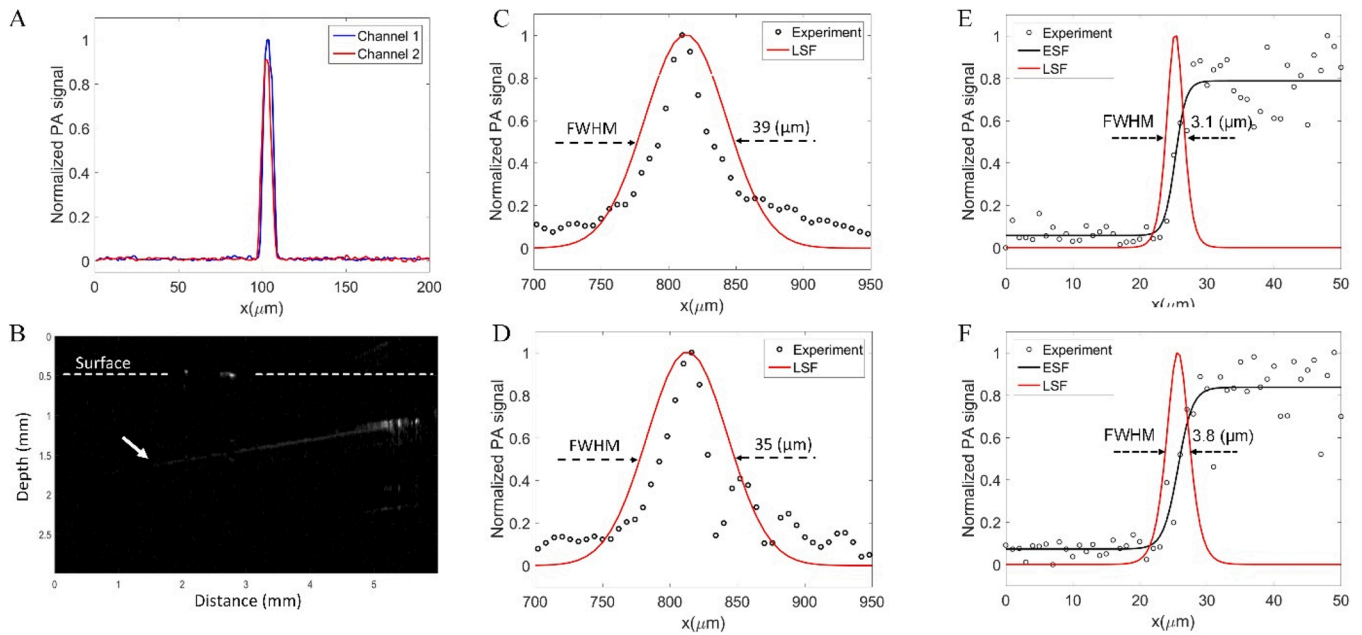
Fig. 3. The SNR, depth penetration, and spatial resolution of CS-2-OR-FPAM. (A) Photoacoustic signal profiles of the carbon fiber images. (B) Cross-sectional PA B-scan image of black tape in chicken tissue. (C) and (D) The axial resolution of channel 1 and channel 2, respectively. (E) and (F) The lateral resolution corresponding to channel 1 and channel 2 of PA probe (see more details in Supplementary Fig. S1).

penetration depth of our CS-2-OR-FPAM was approximately 1.2 mm by imaging the oblique black tape (as the white arrow in Fig. 3B) into fresh breast chicken tissue.

3.3. Ex vivo PA imaging of dragonfly wings

To demonstrate the performance of imaging larger animals, a dead dragonfly's wings were chosen for doing the PA experiment as
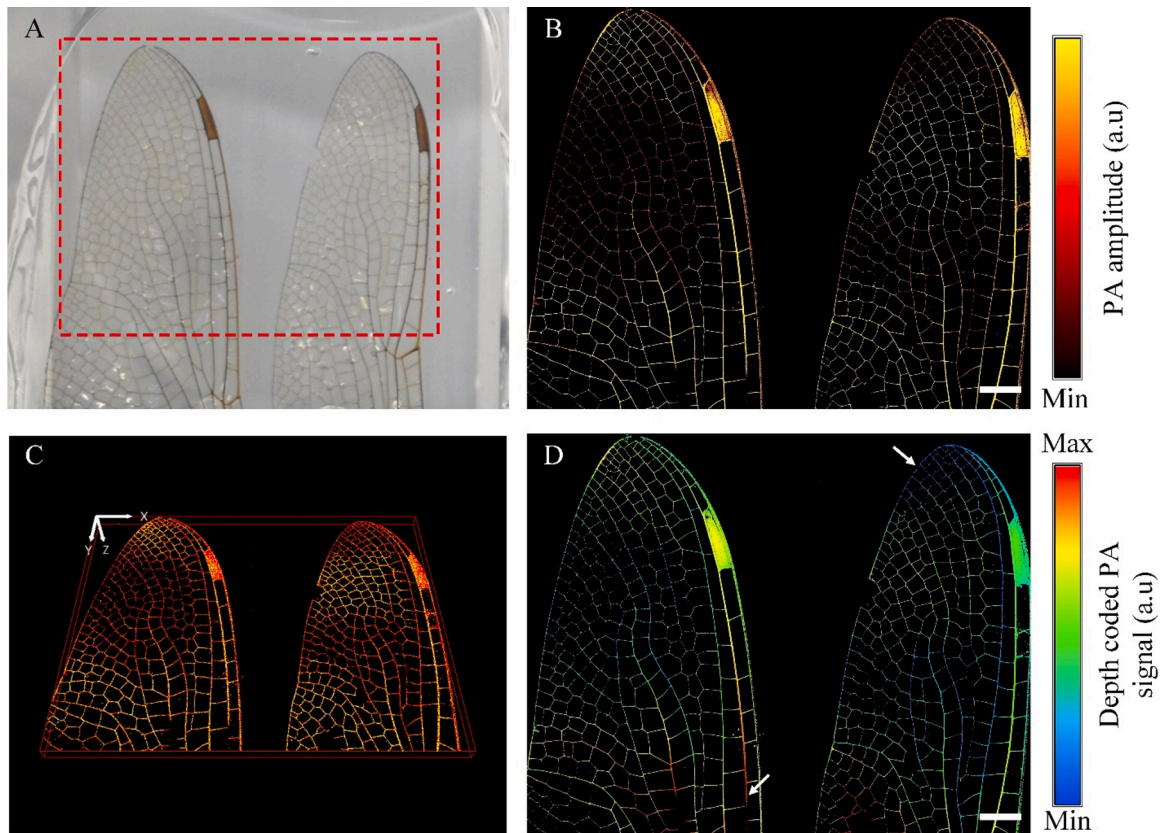

Fig. 4. Photoacoustic (PA) images of a dragonfly's wings *ex vivo*. (A) Photograph of the dragonfly's wings. (B) PA MAP image of the red dash region in (A). (C) The 3D image of the dragonfly's wings. (D) The depth coded PA image of the dragonfly's wings. The scale bar represents 2 mm. (For interpretation of the references to colour in the Figure, the reader is referred to the web version of this article).

illustrated in Fig. 4. The wings have a length of 50 mm and a varying diameter of tubular veins between 1 mm down to less than 0.3 mm. To avoid movement of the wings during scanning, we put them on an acrylic base and then fixed and covered them using an ultrasound gel as a coupling environment. Fig. 4B illustrates the 2-D PA MAP image (imaging range in 24 mm x 19.2 mm and scanning time within 46 s) by the CS-2-OR-FPAM system, and Fig. 4C gives the 3D image of the sample (also see Supplementary Movie 3). These images can characterize the spatial shape and size of the veins in the dragonfly's wings. Based on the depth code PA image, the different depth of the tubular veins was clearly distinguished (highlighted by white arrows in Fig. 4D).

3.4. In vivo PA imaging of a nude mouse ear

To show the possibility of our new imaging system, we successfully imaged microvasculature in the nude mouse ear with the size of 13.7 mm × 6 mm (x- and y- axis, respectively) (Fig. 5). The PA MAP image of the nude mouse ear shows both of artery and vein pairs as well as the capillary beds (as the dash box in Fig. 5B). The volumetric microvasculature image was reconstructed in Fig. 5C, and Supplementary Movie 4.

3.5. In vivo PA imaging of a rat ear

Next, for the larger sample, the microvasculature in a rat ear was clearly defined in a PA MAP image with the wide region (16.8 mm × 10.4 mm along the x- and y- axis, respectively) (Fig. 6). The obtained PA MAP image (Fig. 6B) displays both artery and vein pairs, as well as capillary beds. The volumetric microvasculature image of the rat ear was reconstructed using LabView in Fig. 6C, and Supplementary Movie 5. The blood vessels in the center of the rat ear generated lower PA signals compared to the vessels outside. One possible reason for this difference could be that the thickness of the rat ear. Fig. 6D shows the different thickness of the rat ear by the encoded-depth PA image. The experimental results demonstrated that the system can accomplish the same PA images as the morphology of the blood vessels in a live model (Fig. 6A).

3.6. In vivo enlarged PA imaging of a mouse sagittal

To demonstrate the ultra-widefield FOV of our fast PAM, we obtained the mouse sagittal with a 24 × 20 mm range. Arteries, veins, and microvasculature in the mouse sagittal were observed which shows similar patterns in the mouse ear PA image. (as Fig. 7). The quality of PA image is not good as the nude ear mouse image (or rat ear) due to the thickness of the mouse sagittal (as Fig. 7D).

3.7. In vitro mimicking circulating tumor cells

To demonstrate the advantage of fast scanning capability, we tracked the hemodynamics in the mimicking CTCs using targeted iron oxide nanoparticles as the photoacoustic contrast agent as in Fig. 8 (also see more details in Supplementary Text). The PA signals gradually increased and expanded with time due to the accumulation of iron oxide NPs trapped by the permanent magnetic. The mean PA signal amplitude increases rapidly after applying the permanent magnet at time t = 0. After 15 s, the mean PA signal amplitude is 2.5 times compared with its at 5 s.

4. Discussion

In summary, we designed and fabricated the high-speed OR-PAM system that achieves high SNR over ultra-widefield scanning area. All mechanical, optical components and transducers were integrated into a compact system. Particularly, this slider-crank scanner is relatively cost-effective within $700, and its fabrication process is relatively simple. Although the water-immersible mirror scanners can achieve a high B-scan rate up to ten of hundreds Hz, it has an unstable step size due to the dependence of angular motion, resulting in distortion image. Taking advantage of constant step size by using the linear position module, our SC-2-OR-PAM is not depending on the angular motion. Therefore, the reconstructed PA images is quickly processed without using the interpolated algorithms. The developed system is not only carrying our OAC, it can potentially be used for another OAC which has a better SNR. In comparison with other high-speed PAM systems, we summarized some of the main specifications as in Table 1.

However, there are several restrictions in the current SC-2-OR-PAM. Firstly, the B-scan rate depends on the revolution of the step DC-motor, which have the safe range speed from 0 to 1000 revolution per minute. Our SC-2-OR-PAM converts one revolution to 2 B-scan; thus, the stable B-scan is 32 Hz which is insufficient to imaging the volumetric image in real-time. By using a more powerful DC-motor, it is possible to increase B-scanning rate further. On the other hand, our system can carry dual PA channels even multiple channels to reduce the scanning time over the large FOV for one scan only. Secondly, using two different channels is facing with the different characteristics of their own components such as transducers and optical parts. It is difficult to make two channels with the same SNR and spatial resolutions. Therefore, it will slightly affect to
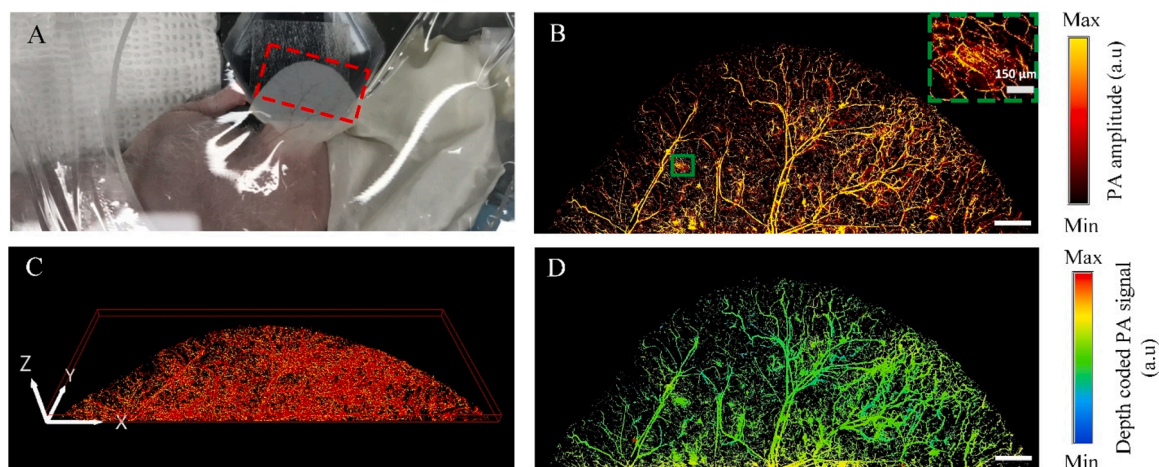

Fig. 5. Photoacoustic (PA) images of a nude mouse ear *in vivo*. (A) Photograph of the nude mouse ear. (B) PA MAP image of the red dash region in (A). (C) The 3D image of the nude mouse ear. (D) The depth-coded PA image of the nude mouse ear. The scale bar represents 1 mm. (For interpretation of the references to colour in the Figure, the reader is referred to the web version of this article).
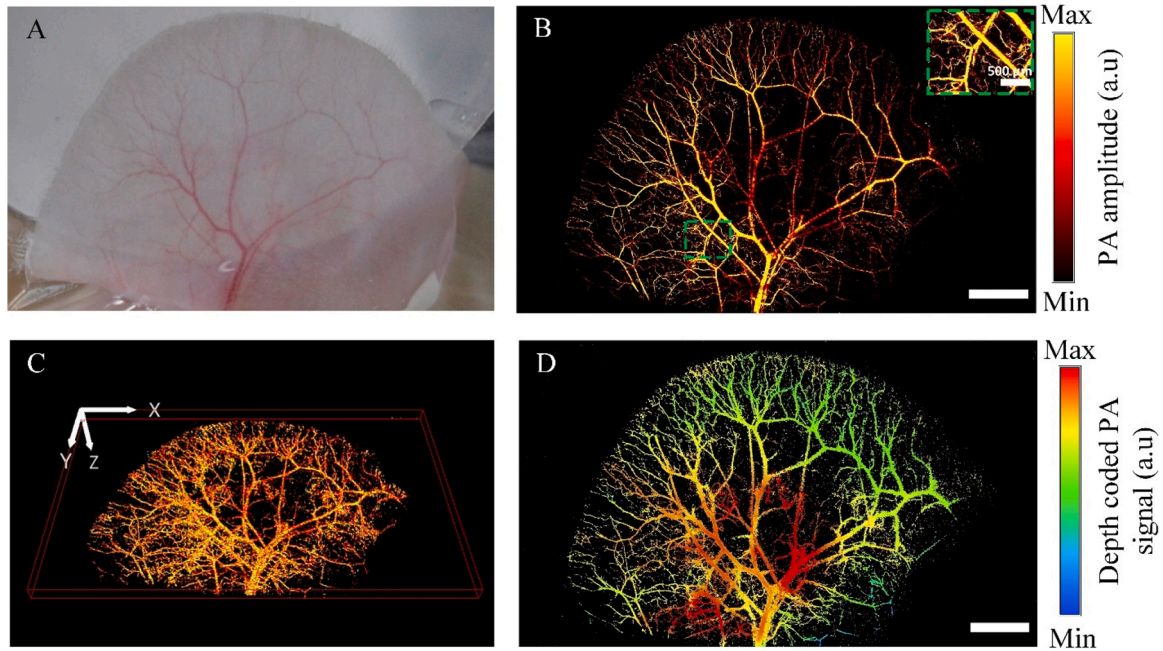
Fig. 6. Photoacoustic (PA) images of a rat ear *in vivo*. (A) Photograph of the mouse ear. (B) PA MAP image of rat ear. (C) The 3D image of the rat ear (also see Supplementary Movie 5). (D) The depth-coded PA image of the rat ear. The length of scale bar is 2 mm.
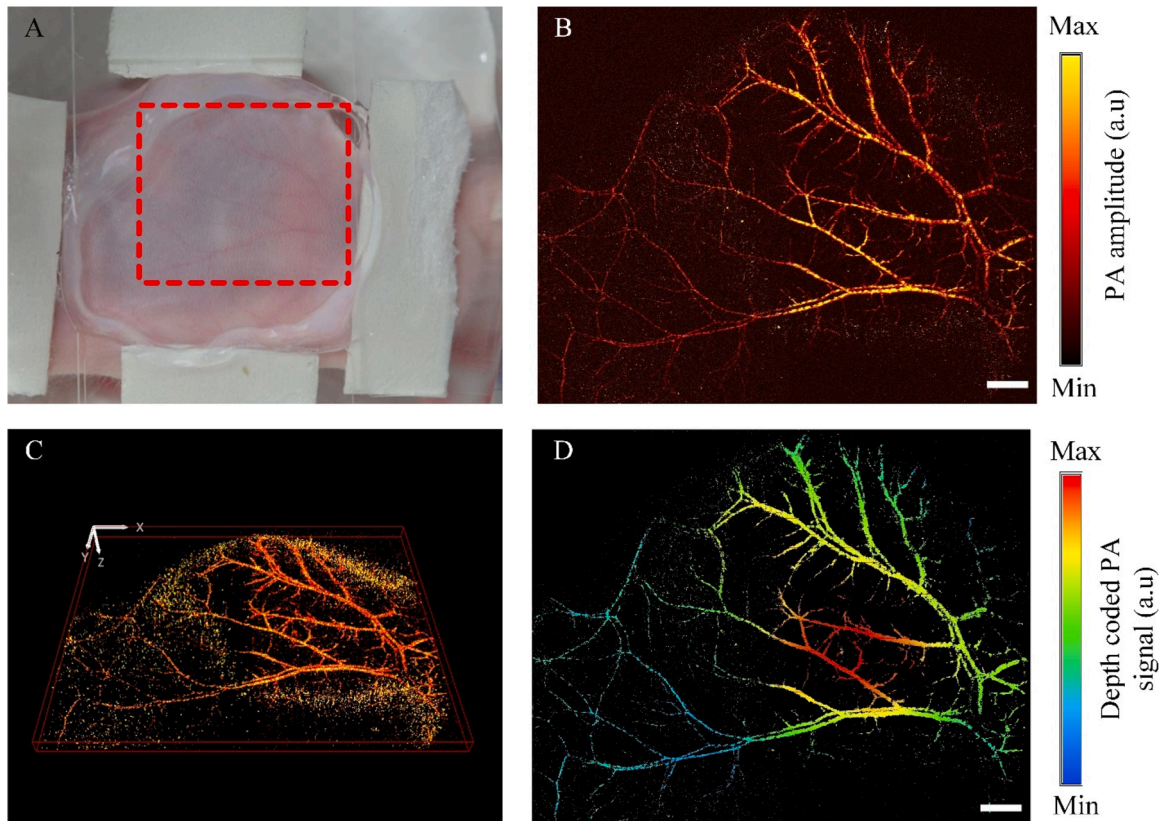

Fig. 7. Photoacoustic (PA) images of a mouse sagittal *in vivo*. (A) Photograph of the mouse sagittal. (B) PA MAP image of the red dash region in (A). (C) The 3D image of the mouse sagittal (also see Supplementary Movie 6). (D) The depth-coded PA image of the mouse sagittal. The scale bar is 2 mm. (For interpretation of the references to colour in the Figure, the reader is referred to the web version of this article).

the quality of the final PA image.

5. Conclusions

In conclusion, using the slider-crank mechanism, we achieved high-speed scanning of up to 32 FPS of B-scan by maintaining a high
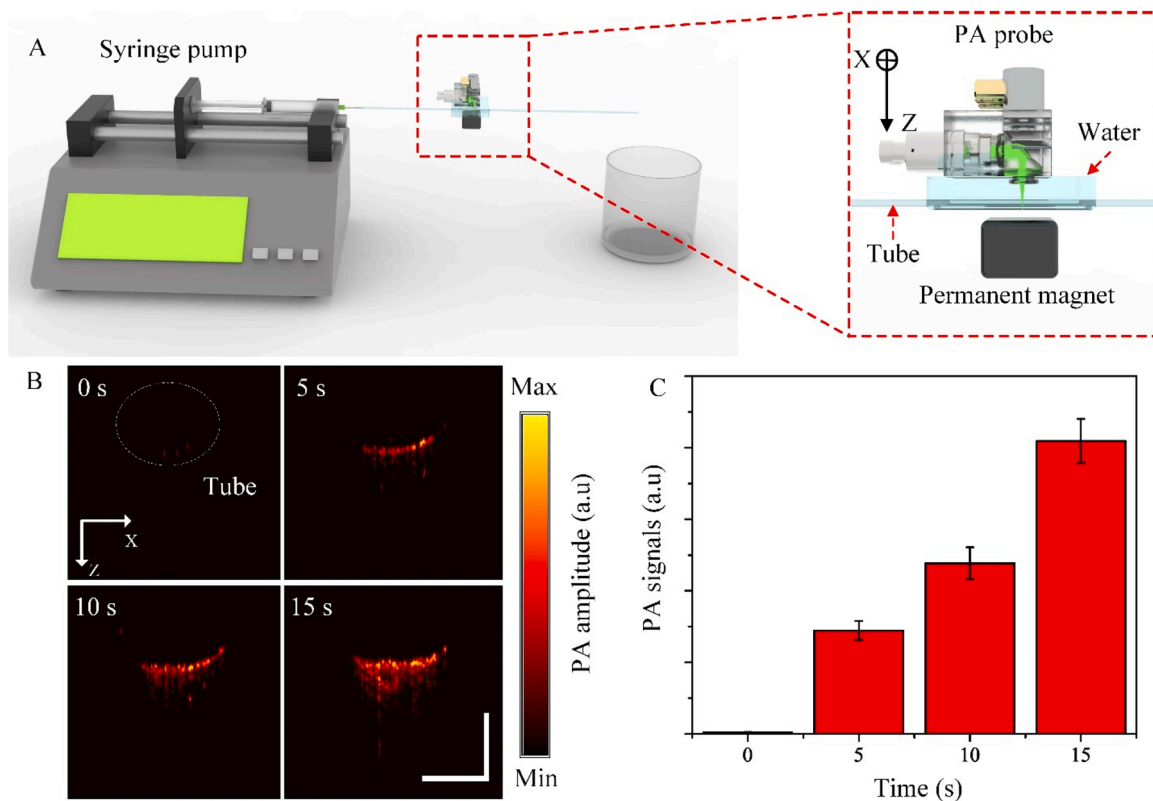
Fig. 8. *In vitro* hemodynamics monitoring in the mimicking CTCs. (A) The configuration of the *in vitro* testing tube. (B) PA B-scan image of the tube in 0 s, 5 s, 10 s, and 15 s (also see Supplementary Movie 7). (C) The PA graph represents the PA signals corresponding to the B-scan image in (B). The scale bar is 1 mm.

Table 1
Specifications of high-speed OR-PAM.

Specifications	Slider-crank scanner	Galvanometer scanner [38]	MEMS scanner [39]	Hexagon-mirror scanner [27]	Voice-coil scanner [29]
Scanning range (fast axis-mm)	24	2.4	3	12	9
B-scan rate (Hz)	32 - 44	500 - 650	400	900	20
Lateral resolution (μm)	3.4	7.5	3	8.8 - 31.9	3.4
Axial resolution (μm)	37	33	15	33	15

resolution, high SNR and ultra-scanning range of up to 12.5 mm (for one channel) or 24 mm (for two channels). The penetration depth, SNR, speed, resolution and FOV were evaluated in phantom and *ex vivo* experiments. The lateral resolution was estimated about at 3.45 μm. We demonstrated the possibilities of our system by imaging various samples, including a dragonfly's wing, a mouse ear, and a mouse sagittal.

Author contribution

V.T.N designed, and developed the OR-PAM system. N.T.P.T programmed the software, analyzed, and interpreted the data, as well as prepared the figures for the manuscript. V.H.P and S.P designed and fabricated the slider-crank mechanism. C.D.L and J.C designed and fabricated the trigger management board for synchronization all devices. V.T.N, S.W.C and S.M performed the experiment. H.G.L revised the manuscript, interpreted the data, and approved the final version. J.O and C.S.K conceived and supervised the project. All authors contributed to critical reading of the manuscript.

Declaration of Competing Interest

The authors declare that there are no conflicts of interest

Appendix A. Supplementary data

Supplementary material related to this article can be found, in the online version, at doi:https://doi.org/10.1016/j.pacs.2021.100274.

References

[1] L.V. Wang, S. Hu, Photoacoustic tomography: in vivo imaging from organelles to organs, Science 335 (6075) (2012) 1458–1462.

[2] J. Yao, L.V.J.L. Wang, p. reviews, Photoacoustic microscopy, Laser Photonics Rev. 7 (5) (2013) 758–778.

[3] N.Q. Bui, S.-W. Cho, M.S. Moorthy, S.M. Park, Z. Piao, S.Y. Nam, H.W. Kang, C.-S. Kim, J.J.Sr. Oh, In vivo photoacoustic monitoring using 700-nm region Raman source for targeting Prussian blue nanoparticles in mouse tumor model, Sci. Rep. 8 (1) (2018) 1–9.

[4] P. Manivasagan, S.W. Jun, G. Hoang, S. Mondal, H. Kim, V.H.M. Doan, J. Kim, C.-S. Kim, J.J.Jocr. Oh, Anti-EGFR antibody conjugated thiol chitosan-layered gold nanoshells for dual-modal imaging-guided cancer combination therapy, J. Controlled Releases 311 (2019) 26–42.

[5] T.T.W. Wong, R. Zhang, P. Hai, C. Zhang, M.A. Pleitez, R.L. Aft, D.V. Novack, L.V. Wang, Fast label-free multilayered histology-like imaging of human breast cancer by photoacoustic microscopy, Sci. Adv. 3 (5) (2017), e1602168.

[6] W. Liu, D.M. Shcherbakova, N. Kurupassery, Y. Li, Q. Zhou, V.V. Verkhusha, J. Yao, Quad-mode functional and molecular photoacoustic microscopy, Sci. Rep. 8 (1) (2018) 11123.

[7] S. Jeon, H.B. Song, J. Kim, B.J. Lee, R. Managuli, J.H. Kim, J.H. Kim, C. Kim, In vivo photoacoustic imaging of anterior ocular vasculature: a random sample consensus approach, Sci. Rep. 7 (1) (2017) 4318.

[8] J.Y. Kim, C. Lee, K. Park, G. Lim, C. Kim, Fast optical-resolution photoacoustic microscopy using a 2-axis water-proofing MEMS scanner, Sci. Rep. 5 (2015) 7932.

[9] D. Lee, S. Beack, J. Yoo, S.K. Kim, C. Lee, W. Kwon, S.K. Hahn, C.J.A.F.M. Kim, In vivo photoacoustic imaging of livers using biodegradable hyaluronic acid-conjugated silica nanoparticles, Adv. Funct. Mater. 28 (22) (2018), 1800941.

[10] D. Lee, C. Lee, S. Kim, Q. Zhou, J. Kim, C.J.Sr. Kim, In vivo near infrared virtual intraoperative surgical photoacoustic optical coherence tomography, Sci. Rep. 6 (2016) 35176.

[11] J. Yao, K.I. Maslov, Y. Shi, L.A. Taber, L.V.J.Ol. Wang, In vivo photoacoustic imaging of transverse blood flow by using Doppler broadening of bandwidth, Opt. Lett. 35 (9) (2010) 1419–1421.

[12] J. Yao, L. Wang, J.-M. Yang, K.I. Maslov, T.T. Wong, L. Li, C.-H. Huang, J. Zou, L.V. J.Nm. Wang, High-speed label-free functional photoacoustic microscopy of mouse brain in action, Nature 12 (5) (2015) 407–410.

[13] S. Park, U. Jung, S. Lee, D. Lee, C. Kim, Contrast-enhanced dual mode imaging: photoacoustic imaging plus more, Biomed. Eng. Lett. 7 (2) (2017) 121–133.

[14] V.P. Nguyen, Y. Li, J. Henry, W. Zhang, M. Aaberg, S. Jones, T. Qian, X. Wang, Y. M. Paulus, Plasmonic gold nanostar-enhanced multimodal photoacoustic microscopy and optical coherence tomography molecular imaging to evaluate choroidal neovascularization, ACS Sens. 5 (10) (2020) 3070–3081.

[15] A. Krumholz, L. Wang, J. Yao, L.V. Wang, Functional photoacoustic microscopy of diabetic vasculature, J. Biomed. Opt. 17 (6) (2012), 060502.

[16] V.H.M. Doan, V.T. Nguyen, J. Choi, S. Park, J.J.A.S. Oh, Fuzzy logic control-based HIFU system integrated with photoacoustic imaging module for ex vivo artificial tumor treatment, Appl. Sci. 10 (21) (2020) 7888.

[17] R. Ma, S. Sontges, S. Shoham, V. Ntziachristos, D. Razansky, Fast scanning coaxial optoacoustic microscopy, Biomed. Opt. Express 3 (7) (2012) 1724–1731.

[18] W. Shi, P. Hajireza, P. Shao, A. Forbrich, R.J.J.Oe. Zemp, In vivo near-realtime volumetric optical-resolution photoacoustic microscopy using a high-repetition-rate nanosecond fiber-laser, Opt. Express 19 (18) (2011) 17143–17150.

[19] E. Zhang, J. Laufer, R. Pedley, P.J.Pi.M. Beard, In vivo high-resolution 3D photoacoustic imaging of superficial vascular anatomy, Biology 54 (4) (2009) 1035.

[20] H. Estrada, J. Turner, M. Kneipp, D.J.L.P.L. Razansky, Real-time optoacoustic brain microscopy with hybrid optical and acoustic resolution, Laser Phys. 11 (4) (2014), 045601.

[21] S. Hu, K. Maslov, L.V. Wang, Second-generation optical-resolution photoacoustic microscopy with improved sensitivity and speed, Opt. Lett. 36 (7) (2011) 1134–1136.

[22] K. Maslov, H.F. Zhang, S. Hu, L.V. Wang, Optical-resolution photoacoustic microscopy for in vivo imaging of single capillaries, Opt. Lett. 33 (9) (2008) 929–931.

[23] T.J. Allen, J. Spurrell, M.O. Berendt, O. Ogunlade, S.U. Alam, E.Z. Zhang, D. J. Richardson, P.C.J.Jo.B.O. Beard, Ultrafast laser-scanning optical resolution photoacoustic microscopy at up to 2 million A-lines per second, J. Biomed. Optics 23 (12) (2018), 126502.

[24] Z. Xie, S. Jiao, H.F. Zhang, C.A.J.Ol. Puliafito, Laser-scanning optical-resolution photoacoustic microscopy, Opt. Lett. 34 (12) (2009) 1771–1773.

[25] Y. Yuan, S. Yang, D.J.A.P.L. Xing, Optical-resolution photoacoustic microscopy based on two-dimensional scanning galvanometer, Appl. Phys. Lett. 100 (2) (2012), 023702.

[26] J.Y. Kim, C. Lee, K. Park, S. Han, C. Kim, High-speed and high-SNR photoacoustic microscopy based on a galvanometer mirror in non-conducting liquid, Sci. Rep. 6 (2016) 34803.

[27] B. Lan, W. Liu, Y.-c. Wang, J. Shi, Y. Li, S. Xu, H. Sheng, Q. Zhou, J. Zou, U.J.B.o. e. Hoffmann, High-speed widefield photoacoustic microscopy of small-animal hemodynamics, Biomed. Opt. Express 9 (10) (2018) 4689–4701.

[28] J. Chen, Y. Zhang, L. He, Y. Liang, L.J.P. Wang, Wide-field polygon-scanning photoacoustic microscopy of oxygen saturation at 1-MHz A-line rate, Photoacoustics (2020), 100195.

[29] L. Wang, K. Maslov, J. Yao, B. Rao, L.V. Wang, Fast voice-coil scanning optical-resolution photoacoustic microscopy, Opt. Lett. 36 (2) (2011) 139–141.

[30] S. Jeon, J. Kim, D. Lee, J.W. Baik, C.J.P. Kim, Review on practical photoacoustic microscopy, Photoacoustics 15 (2019), 100141.

[31] D. Li, C. Liu, Y. Yang, L. Wang, Y.J.L.S. Shen, Micro-rocket robot with all-optic actuating and tracking in blood, Applications 9 (1) (2020) 1–10.

[32] B. Rao, L. Li, K. Maslov, L. Wang, Hybrid-scanning optical-resolution photoacoustic microscopy for in vivo vasculature imaging, Opt. Lett. 35 (10) (2010) 1521–1523.

[33] P. Hajireza, W. Shi, R.J. Zemp, Label-free in vivo fiber-based optical-resolution photoacoustic microscopy, Opt. Lett. 36 (20) (2011) 4107–4109.

[34] W. Qin, T. Jin, H. Guo, L. Xi, Large-field-of-view optical resolution photoacoustic microscopy, Opt. Express 26 (4) (2018) 4271–4278.

[35] O. Liba, M.D. Lew, E.D. SoRelle, R. Dutta, D. Sen, D.M. Moshfeghi, S. Chu, A. de la Zerda, Speckle-modulating optical coherence tomography in living mice and humans, Nat. Commun. 8 (2017) 15845.

[36] B.G. Saar, C.W. Freudiger, J. Reichman, C.M. Stanley, G.R. Holtom, X.S. Xie, Video-rate molecular imaging in vivo with stimulated Raman scattering, Science 330 (6009) (2010) 1368–1370.

[37] A.M. Packer, L.E. Russell, H.W. Dalgleish, M. Hausser, Simultaneous all-optical manipulation and recording of neural circuit activity with cellular resolution in vivo, Nat. Methods 12 (2) (2015) 140–146.

[38] J. Kim, J.Y. Kim, S. Jeon, J.W. Baik, S.H. Cho, C.J.L.S. Kim, Super-resolution localization photoacoustic microscopy using intrinsic red blood cells as contrast absorbers, Applications 8 (1) (2019) 1–11.

[39] C. Lee, J.Y. Kim, C. Kim, Recent progress on photoacoustic imaging enhanced with microelectromechanical systems (MEMS) technologies, Micromachines (Basel) 9 (11) (2018).

[40] K. Hwang, Y.-H. Seo, K.-H.J.M. Jeong, Microscanners for optical endomicroscopic applications, N.S. Letters 5 (1) (2017) 1–11.
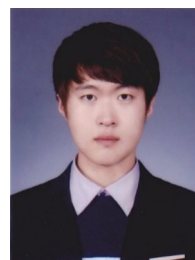
Van Tu Nguyen received the M.Sc. degree in Biomedical Engineering from Pukyong National University, Republic of Korea in 2018. He is currently doing pH.D. degree in Biomedical Engineering, Pukyong National University. His research focuses on biomedical imaging methods, including photoacoustic imaging and fluorescence imaging.

Nguyen Thanh Phong Truong received the B.S. degree in Biomedical Engineering from University of Technology, Ho Chi Minh city, Vietnam, and the M.S. degree in Biomedical Engineering from Pukyong National University, Busan, South Korea, in 2013 and 2019, respectively. After getting B.S. degree, he joined Olympus Medical System Vietnam, a part of Olympus Corporation, Japan for 4 years. He is currently doing pH.D. degree in Biomedical Engineering, Pukyong National University. His current research interests include scanning acoustic microscopy and photoacoustic imaging.

Hiep Pham Van received the B.S. degree in Mechanical Engineering from Hanoi University of Sience and Technology, HaNoi, Vietnam, and the M.S. degree in Biomedical Engineering from Pukyong National University, Busan, South Korea, in 2010 and 2020, respectively. After getting B.S. degree, he worked at Z43 company as technical assistant for 2 years. He is currently doing pH.D. degree in Biomedical Engineering, Pukyong National University. His current research interests include scanning acoustic microscopy and microstructure properties.

Jaeyeop Choi received the B.S. and M.S. degree in Biomedical Engineering from Pukyong National University, Busan, Republic of Korea. He is currently doing pH.D. degree in Industry 4.0 Convergence Bionics Engineering, Pukyong National University. His current research interests include high frequency ultrasonic transducer and scanning acoustic microscopy.

Sumin Park received the B.S. degree in Biomedical engineering, Pukyong National University, South Korea (2020). She is currently pursuing her M.S. degree in Industry 4.0 Convergence Bionics Engineering, Pukyong National University, South Korea. Her research interests include fabrication of the transducers, Scanning Acoustic Microscopy, hydroxyapatite and nanoparticles.

Hae Gyun Lim received his B.S. degree in biochemistry from University of California, Los Angeles, CA in 2010. He obtained his M.S. and pH.D. degrees in biomedical engineering from University of Southern California, Los Angeles, CA in 2014 and 2017, respectively. From 2013 through 2017, he was a Research Assistant for the NIH Resource Center for Medical Ultrasonic Transducer Technology. Dr. Lim worked as a Postdoctoral Research Associate for the Future IT Innovation Laboratory at Pohang University of Science and Technology (POSTECH), Pohang, Korea from 2017 to 2021. Dr. Lim currently works as assistant professor at Pukyong National University. His research interests include ultrasonic transducers, cell manipulation, and high frequency ultrasound microbeams.

Cao Duong Ly has recently received the master's degree in Biomedical Engineering after graduating from Pukyong National University, Republic of Korea. He is currently working as a system engineer and research assistant in Nano Bio Medicine Lab, Department of Biomedical Engineering, Pukyong National University. His research focuses on biomedical electronics and biomedical imaging areas in ultrasonic imaging, photoacoustic imaging and fluorescence imaging.

Chang-Seok Kim received the pH.D. degree from The Johns Hopkins University, Baltimore, MD, USA, in 2004. He is a Professor with the Department of Optics and Mechatronics Engineering and the Department of Cogno-Mechatronics Engineering, Pusan National University, Busan, South Korea. His current research interests include the development of novel fiber laser systems and application of them into biomedical, telecommunication, and sensor areas.

Soon-Woo Cho received the M.S. degree from the Department of CognoMechatronics Engineering, Pusan National University, Busan, South Korea, in 2016. She is currently working toward the pH.D. degree at the Department of Cogno-Mechatronics Engineering, Pusan National University. Her current research interests include the development of novel fiber laser system and optical imaging system for biomedical applications.

Junghwan Oh received the B.S. degree in Mechanical engineering from Pukyong National University in 1992, and the M.S. and pH.D. degrees in Biomedical engineering from The University of Texas at Austin, USA, in 2003 and 2007, respectively. In 2010, he joined the Department of Biomedical Engineering at Pukyong National University, where he is a Full Professor. He also serves as Director of OhLabs Corporation research center. His current research interests include ultrasonic-based diagnostic imaging modalities for biomedical engineering applications, biomedical signal processing and health care systems.

Sudip Mondal obtained his PhD in 2015 from CSIR-Central Mechanical Engineering Research Institute and National Institute Technology Durgapur, India. He joined as a Post-Doctoral Fellow at Benemérita Universidad Autónoma de Puebla (BUAP) University, Mexico (2015–2017). Currently he works as Research Professor, at the Department of Biomedical Engineering, in Pukyong National University, South Korea. His research interests include nanostructured materials synthesis, bioimaging, and biomedical applications such as cancer therapy and tissue engineering.